

Optimal Design Parameter Determination for Brushless Doubly Fed Induction Machines

M. Yousefian, H. Abootorabi Zarchi, S. Abdi, H. Gorginpour

Abstract – Brushless doubly fed induction machines (BDFIM) have prominent features for variable speed applications. The design and performance analysis of the machine is however complex compared to the conventional induction machines due to its special magnetic fields generated from two stator winding with different pole numbers and frequencies. In this paper, the effective parameters in BDFIM design and their limitations are investigated. In relation with the design objectives, control variables are identified, and an optimal prototype machine design is proposed. The results from experimental tests and finite element simulations of a 3 kW prototype BDFIM are presented to assess the effectiveness of the proposed parameters determination method.

Index Terms-- Brushless doubly fed induction machine, Finite element analysis, Nested-loop rotor, Design variables.

I. INTRODUCTION

THE brushless doubly fed induction machine (BDFIM) is a variable speed machine with attractive features for both motor and generator applications. The most important advantage of BDFIM is that it does not require brushes and slip rings reducing its repairs and maintenance costs. In addition, in variable speed operation it can operate at a higher power factor than induction motors using only a fractional-sized converter, leading to significant economic benefits [1]. Another advantage for the BDFIM is the possibility of operating as a conventional induction machine when an error occurs in the converter. The machine is especially attractive to be used as wind generator as a replacement to the well-known doubly fed induction generators (DFIG) [2].

The BDFIM also has significant advantages, especially for coastal and remote locations due to its high reliability and low maintenance requirements [3]. As a motor and due to partially-rating converter requirement, it is a suitable machine for the pump and fan start up [4] since the fluid loads do not require high starting torque.

Due to the high cost of rare magnetic materials used in permanent magnet machines, and the advances in controllability of the BDFIM, research has also been conducted on the use of BDFIM in automotive applications. In [5] a comparison between a brushless doubly fed induction generator and a claw-pole generator for in-vehicle use is shown and the superiority of BDFIM was shown in terms of

efficiency at higher speeds. Several patents have been made for various applications of BDFIM, as a generator for use in offshore wind turbines [4], hydro plants with low altitude [6], and for vehicles [7]. The BDFIM can also be used for the ships' electrical power generation [8].

To design and construct a BDFIM, it is necessary to pay special attention to its effective design parameters. In this paper and based on the design objectives, control variables are identified, and an optimal prototype design is proposed. The results from experimental tests and finite element simulations are presented in induction mode. Also, the harmonic spectrum of the air gap flux density is extracted in cascade induction mode. There are only a few references with special focus on BDFIM design and therefore, there is still a need for more research on design optimisation. In [9] the design and electromagnetic behavior of the BDFIM rotor were studied. Two machines with 4/8 pole stator windings, have been used with different sizes D180 and D160. The results showed that the rotor winding and core design are important for the desirable performance. In [10] and [11], design optimisation of the BDFIM were discussed. In these works, conventional design procedure was used as for the standard induction machine with specific aim at maximising the output torque. In [12] The BDFIM equivalent circuit model was approximated where the core losses and leakage reactances of the stator windings were ignored. However, the lamination geometries and thickness were fixed and hence were not part of the calculation process.

II. BRUSHLESS DOUBLY FED INDUCTION MACHINE

The brushless doubly fed machine requires two alternating power supplies and there is no direct electrical connection between the rotor and its stator. One of the stator windings is directly connected to the grid called power winding (PW) and hence has a constant frequency. The other winding is connected to the grid through a back-to-back converter with a partial rating, called the control winding (CW). The number of pole pairs of these windings must be selected in a way to prevent direct magnetic couplings [5]:

$$|p_P - p_C| > 1 \quad (1)$$

where p_C and p_P are the PW and CW pole pairs, respectively. The BDFIM rotor has $p_r = p_P + p_C$ poles, called nests, that are equal to the sum of the pole pair numbers [13]. Each nest usually contains 3 to 5 loops. Fig. 1 shows the BDFIM winding arrangements.

A. Induction and Cascade Modes of Operation

Induction mode can be achieved if one of the stator windings is opened and the other is supplied. The machine will hence operate as an induction machine with reduced

M. Yousefian is with the Department of Electrical Engineering, Technical and Vocational University (TVU), Tehran, Iran (e-mail: mahmoud.yousefian@yahoo.com).

H. Abootorabi Zarchi is with Engineering Department, Faculty of Engineering, Ferdowsi University of Mashhad, Mashhad, Iran (e-mail: abootorabi@um.ac.ir).

S. Abdi jalebi is with the Engineering Department, University of East Anglia, Norwich, UK (e-mail: S.abdi-jalebi@uea.ac.uk).

H. Gorginpour is with Engineering Department, Persian Gulf University, Bushehr, Iran (e-mail: ha.gorgin@gmail.com).

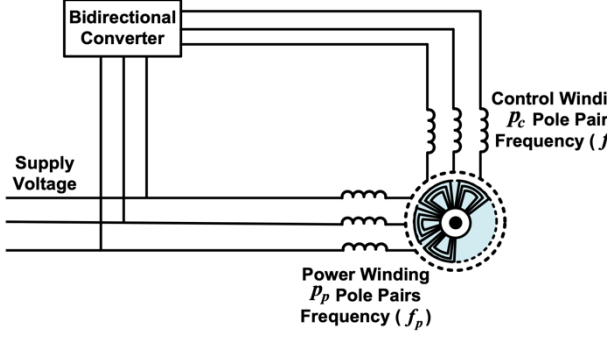


Fig. 1. Brushless doubly fed induction machine's winding connections

effective performance.

In cascade mode, one stator winding is supplied, and the other winding is shorted. In this mode, the magneto motive force generated by the supplied winding induces an emf in the rotor bars which in turn result in the production of the emf in the rotor consisting of harmonics with p_p and p_c pole pairs. In this mode, the mechanical power produced by the machine has two terms: One is similar to the mechanical power of an induction machine with p_p pole pairs and the other is similar to an induction machine with p_r pole pairs [14]. This results in the machine operation in two stable active regions around the synchronous speeds with p_p and p_r pole pairs.

B. Synchronous Mode of Operation

The synchronous mode is the most desirable mode of operation for the BDFIM. In this mode, both PW and CW are fed. The CW is powered by a partial capacity converter whose current or output voltage amplitude is adjusted according to operating conditions. Depending on the phase sequence of the control winding, there are two types of sub-synchronous and super-synchronous operations [15]. The fundamental magnetic fields are generated in the air gap as:

$$B_p(t, \theta_p) = B_{p,max} \cos(\omega_p t - p_p \theta_p) \quad (2)$$

$$B_c(t, \theta_c) = B_{c,max} \cos(\omega_c t - p_c \theta_c) \quad (3)$$

where θ_p and θ_c are the spatial angles around the air gap for the PW and CW, respectively. The rotational speeds of the fields depend on the windings' supplied frequencies and their poles numbers. To produce non-zero average torque, the currents induced in the rotor by these two fields must have the same frequency and distribution. To achieve this, the number of rotor poles is determined by the following equation:

$$p_r = p_p \pm p_c \quad (4)$$

where p_r is the number of rotor nests. To reduce the harmonic content of the rotor magnetic field, the nests are designed having several loops [13]. The rotor speed can be obtained from:

$$\omega_r = \frac{\omega_p + \omega_c}{p_p + p_c} \quad (5)$$

III. PARAMETERS AND CONSTRAINTS IN BDFIM DESIGN

In this section, the main parameters and constraints in the BDFIM design are investigated. Also, control variables are identified for optimal design based on the available information and design objectives. The objective function is defined according to the optimal design of the stator windings and the nested loop rotor. The stator with specified dimensions is designed for a 460 V induction motor, 4-poles, 132 frame size and an output power of 5800 W. In [16], the effective parameters are well presented for the output equation of induction machines. In the following, control variables and design constraints are determined, taking also into account the construction limitations

A. The Number of Poles of PW and CW

There are several works reported on the suitable and optimal determination of the number of poles in a conventional induction machine [17]. The BDFIM's speed range is within $\pm 30\%$ of its natural speed and hence it has a lower speed range than a conventional induction machine, leading to less expensive gearbox system. In this study, a 2/4 pole pair combination is considered as one of the most widely used stator windings design reported in the literature [18].

B. PW and CW Voltages

In induction typed machines, the voltage is usually suggested based on its power, according to the related IEC standards. In this work and based on the available stator core and the presence of nominal fluxes caused by the two stator windings, the PW and CW voltages have been determined to be 180 and 200 V, respectively. Also, the nominal frequency of both windings is chosen to be 50 Hz.

C. Stator Windings Connections

The star connection has been used for stator windings due to the lower voltage value across each phase. To reduce the spatial harmonic distortion in the air gap, two-layer winding is used with fractional pitch. The specifications of the power and control windings are given in Table I.

D. Geometric Structure of Stator and Rotor

In stator and rotor design of induction machines, the magnetic core cross section shape varies depending on the power ratings. Semi-closed slots at low power and open slots at high power are often used. To increase the cross-section area of the slots the teeth are selected in parallel, especially for the stator. Aluminum diecast or copper bar is often used

TABLE I
THE WINDING SPECIFICATIONS FOR STATOR PW AND CW

	Coil pitch	Winding Type	Connecting coil groups	Connection type
PW	10	two-layer, fractional pitch, chain winding	Series, far connection	Star
CW	5	two-layer, fractional pitch, chain winding	Series, far connection	Star

TABLE II
NUMBER OF POSSIBLE SLOTS FOR A 6-POLE NESTED LOOP ROTOR

Number of rotor nests (p_r)	Number of loops in the nest (N_{rl})	Number of rotor slots (N_{rs})
6	1	12
6	2	24
6	3	36
6	4	48
6	5	60

in cage rotors. Fig. 2 shows the geometric structure of the available stator for the design of the prototype BDFIM. Determining the number of rotor nests is important for the initial design. Since the number of rotor poles is equal to the sum of pole pairs of two stator windings, the rotor should have 6 nests. The constraint on the construction of the rotor core sheet must be considered in selecting the number of loops in each nest. Table II shows the number of possible slots for a 6-pole nested loop rotor.

Based on the slot combinations and the condition of the BDFIM magnetic fields harmonics presented in [19], 48/36 stator/rotor slot combination has been chosen in this study. The number of loops per nest (N_{rl}) can hence be obtained:

$$N_{rl} = \frac{N_{rs}}{2p_r} \quad (6)$$

which is 3 for the machine considered.

It is difficult to construct skewed bars for a nested loop arrangement with copper diecast rotor bars as the rotor bars must be insulated against the rotor core. The production of copper bars with a trapezoidal cross-section is also complex. In addition, insulation of the bars surface and their placement in the slot makes the implementation process more complicated. Therefore, rectangular and parallel rotor slot cross-section is considered in this work. Fig. 3 shows the geometric structure of the rotor sheet and the main geometrical parameters for the optimal design consideration. The relationships between these parameters are shown in (7).

$$\begin{cases} D_{r_o} = D_{s_i} - 2g \\ D_{r_i} = D_{s_i} - 2g - 2h_{rs} - 2h_{r_y} - 2h_{rs_o} \\ w_{rst1} = \frac{\pi(D_{s_i} - 2g - 2h_{rs_o} - 2h_{rs})}{N_{rs}} - w_{rs} \\ w_{rst2} = \frac{\pi(D_{s_i} - 2g - 2h_{rs_o})}{N_{rs}} - w_{rs} \end{cases} \quad (7)$$

The independent design variables that play a main role in optimising the geometric structure are given in Table III. Some references have provided experimental relationships to

TABLE III
GEOMETRIC CONTROL VARIABLES IN DESIGN OPTIMISATION PROCESS

rotor slot depth	rotor yoke height	rotor slot width	air gap length
h_{rs}	h_{r_y}	w_{rs}	g

calculate air gap length. In [20] the calculation of the air gap length in BDFIM is given by the following equation.

$$g \geq \frac{\pi D_{s_i}}{p_p} \times 10^{-3} \quad (8)$$

where i is the inner diameter of the stator in mm and p_p is the number of PW pole pairs, leading to the air gap length of $g = 0.21$ mm for the machine considered. However, (8) is not accurate for power ratings less than 10 kW. Considering the dimensions and power of the machine, and the amount of looseness required by the bearings, the air gap length is selected to be 0.3 mm. Another design constraint is the size of the shaft diameter to withstand the maximum torsional torque applied to it. The width of the stator slot is limited to a maximum of 0.7 slot pitch. In rotors with copper bars, the width of the rotor slot may be less than 0.3 slot pitch. Tooth width is another limitation of the core sheet fabrication. The higher the slot height, the higher the tooth width should be. Table IV shows the dimensional constraints of the rotor core sheet.

E. Converter Rating

When BDFIM speeds away from the natural synchronous

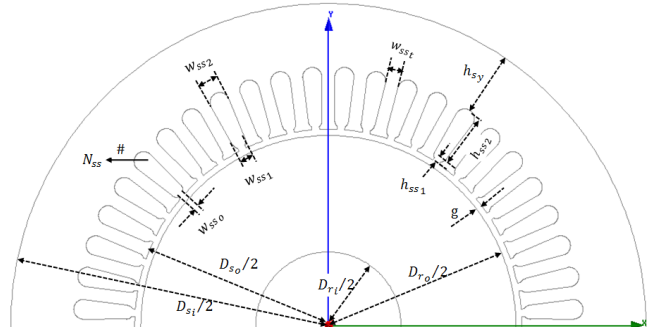


Fig. 2. geometric structure of the stator

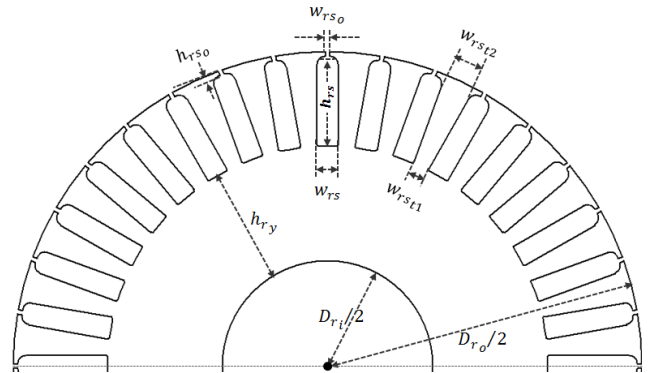


Fig. 3. geometric structure of the rotor

TABLE IV
DIMENSIONAL CONSTRAINT OF ROTOR CORE SHEET

Tooth width at the bottom (mm)	Slot width ratio to rotor slot pitch	Shaft diameter (mm)	air gap length (mm)
$w_{rst1} \geq 3.9$	$0.5 \geq \frac{w_{rs}}{T_{rs}} \geq 0.28$	$D_{r_i} \geq 40$	$g \geq 0.3$

speed, the converter should handle a larger power. Due to the processing of two powers through the air gap and the reduction of the CW power factor, the power of the BDFIM converter must be chosen to be larger than the brushed doubly fed induction machine. The converter rating hence depends on the speed range and the economic considerations. For example, if the speed range is around $\pm 30\%$ of the natural speed, the converter rating should be in the range of 25% - 45% of the PW capacity. In [5] it is shown that the converter rating also depends on the number of poles of two stator windings. In this research, converter rating is limited to a maximum of 35% of the PW rating.

F. Insulation Class

The insulation class of an electric machine depends on the operating conditions, the temperature rise at different parts of the machine, and the insulation type. Thermal analysis in electric machines has not yet reached sufficient maturity. The processes used in conventional induction machines can also be used to study the temperature profile in the BDFIM. It is often possible to ensure that the temperature rise is within the allowable range by observing design constraints. The simulation results showed that for a BDFIM it is advisable to consider the minimum insulation class F and H for the stator and rotor windings, respectively. Kapton insulation tape has been used for rotor bars. The final insulation is done by Global VPI (vacuum pressure impregnation) method. The final temperature of the winding with respect to the machine volume were assessed by considering different sources of heat generation using the recommended processes presented in [21], and different levels of insulation have been proposed accordingly for the prototype BDFIM.

G. Magnetic and Electric constraints

The choice of flux density in different parts of the core plays a very important role in the values of rating, power factor, no-load current, and core losses. Depending on the tooth flux density and the size of the machine, specific magnetic loading has been presented in different sources in the range of 0.3 to 0.8 Tesla. This is often between 0.4 and 0.65 Tesla for 50 Hz induction machines. In BDFIM both the flux density of the PW and CW are present in the core. In [9] (9) has been proposed to determine the BDFIM's magnetic loading based on the PW and CW flux density values:

$$\bar{B} = \frac{2\sqrt{2}}{\pi} \sqrt{B_p^2 + B_c^2} \quad (9)$$

TABLE V
ALLOWABLE FLUX DENSITY RANGES

Section	Flux density range (T)	Maximum flux density (T)
Air gap	0.4-0.65	
Stator yoke	1.1-1.6	1.7
Stator tooth	1.4-1.8	2.1
Rotor yoke	1.2	1.7
Rotor tooth	1.5-2	2.2

The permissible flux density values in different parts of the core are expressed in Table V according to IEC 60404-8 and the saturation curve of usual magnetic sheets.

In the studied machine, magnetic steel sheets with M470-50A grade have been used. The B-H curve for the iron core must be known to ensure the results of finite element analysis are accurate. In addition, the mesh intensity in the critical areas such as air gap and rotor and stator teeth must be carefully considered to accurately predict the effects of saturation.

Specific electric loading on the PW and CW can be determined from the following equations, respectively [13]:

$$\bar{J}_p = \frac{6N_{ph_p}k_{wp}|I_p|}{\pi D_{s_i}} \quad (10)$$

$$\bar{J}_c = \frac{6N_{ph_c}k_{wc}|I_c|}{\pi D_{s_i}} \quad (11)$$

where N_{ph_p} and N_{ph_c} are the PW and CW number of turns per phase, respectively. The current density limit for the rotor is considered similar to that of the stator windings.

IV. DETERMINATION OF THE OBJECTIVE FUNCTION AND DESIGN ALGORITHM

The objective function can be itemised into several objectives such as cost minimization, losses, rotor winding leakage inductance, voltage regulation percentage, output power maximisation, CW power factor, torque, power to weight ratio, or a combination of these objectives. In this research, the simultaneous objective function includes minimising the rotor leakage inductance and maximising the efficiency and power factor of the control winding. Reduction of rotor leakage inductance can lead to a decrease in rotor harmonic components. The objective function is therefore as follows:

$$\text{Objective Function} = \min \left[\frac{(L_r)}{(P.F_{cw})(\eta)} \right] \quad (12)$$

where η is efficiency, L_r is rotor leakage inductance and $P.F_{cw}$ is CW power factor.

Due to the dependency of the objective function components to the equivalent circuit parameters, it is necessary to calculate the equivalent circuit parameters of the machine at steady state. In this paper, the coupled circuit model described in [22] is used. Sensitivity analysis has been performed for all control variables. The results show that the control variables have a significant effect on the components of the objective function. Fig. 4 shows the optimal design flowchart.

V. FINITE ELEMENT AND EXPERIMENTAL ANALYSIS OF THE PROTOTYPE BDFIM

The results from the optimal design procedure with taking the design limitations into account are shown in Table VI. A BDFIM prototype was constructed based on the results

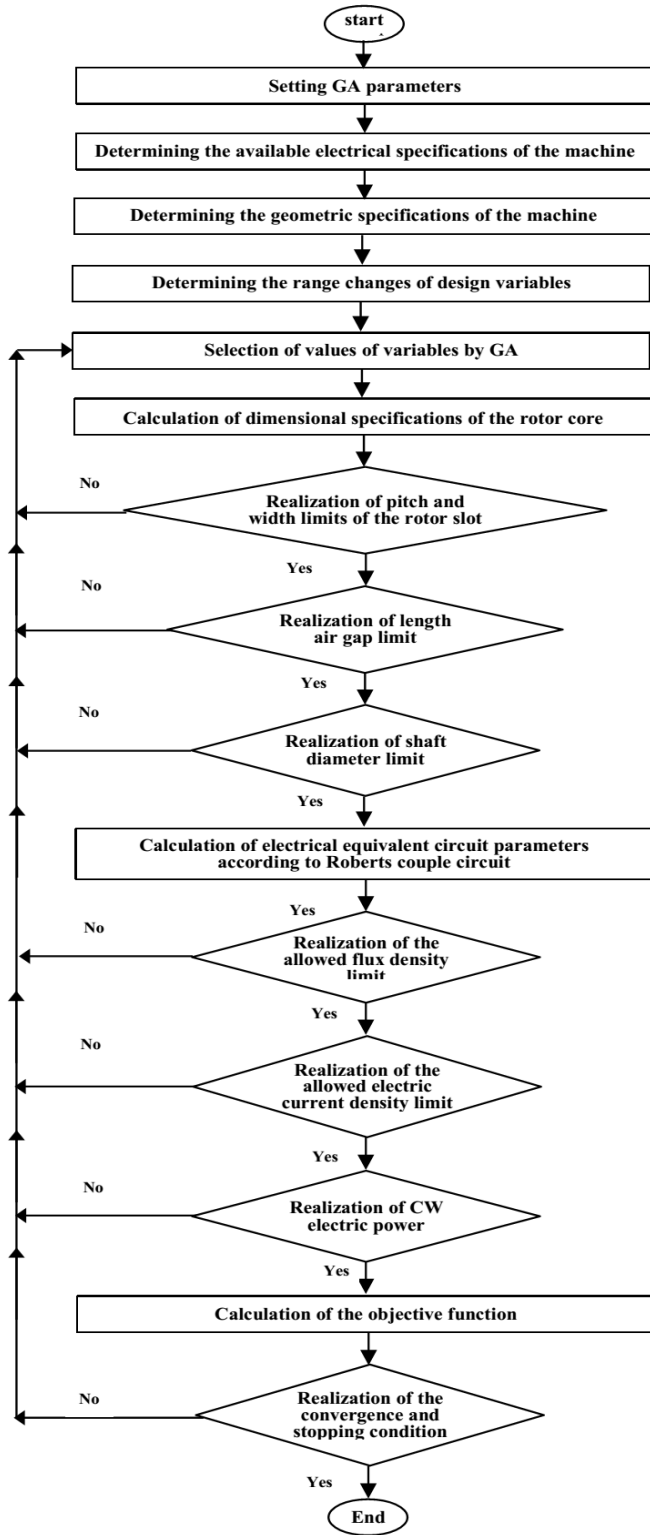


Fig. 4. Optimal BDFIM design flowchart

obtained from the optimal design and shown in Fig. 5. The static and the insulation resistance tests as well as the vibration test were carried out in induction mode of operation and the test results were satisfactory. To evaluate the starting and no-load currents and the generated flux density, the machine was tested at PW and CW induction modes and no-load conditions. The test results have been compared with

the FE simulation in Table VII.

TABLE VI
OPTIMAL DESIGN PARAMETERS OF THE BDFIM CONSIDERED IN THIS STUDY

Description	Parameter	Value
Air gap length	g	0.32 mm
Rotor slot depth	h_{rs}	20.70 mm
Rotor yoke height	h_{s_y}	17.48 mm
Rotor slot width	w_{rs}	3.25 mm
Number of turns per coil of PW	N_{1p}	13
Number of turns per coil of CW	N_{1c}	24
Effective current of PW	I_p	8.2
Effective current of CW	I_c	3.8
Rotor outer diameter	D_{r_o}	127.36 mm
Rotor inner diameter (shaft diameter)	D_{r_i}	48 mm
Tooth width at the bottom	w_{rst1}	4 mm
Tooth width at the top	w_{rst2}	7.60 mm
Copper loss	P_{cu}	750 W
Total loss	ΔP	920 W
Power capacity of CW	P_{cw}	868 W
Power factor of CW	$P.F_{cw}$	0.658
Rotor leakage inductance at stator side	L'_r	0.0206 H
Efficiency	$\% \eta$	$\%66.7$
Objective function value	$O.F$	$3.918e(-6)$
Rated torque	T_n	25.9 Nm
Magnetic loading	\bar{B}_g	0.586

TABLE VII
COMPARISON OF THE PW/CW PARAMETER VALUES OBTAINED FROM THE SIMULATION AND EXPERIMENTS

Winding	Experiment / Simulation	Power factor	Current (A)	Power (W)	Speed (rpm)
PW	Experiment	0.16	1.97	95	1495
	Simulation	0.15	1.90	91	1495
CW	Experiment	0.17	1.99	118	749
	Simulation	0.17	1.80	112	749

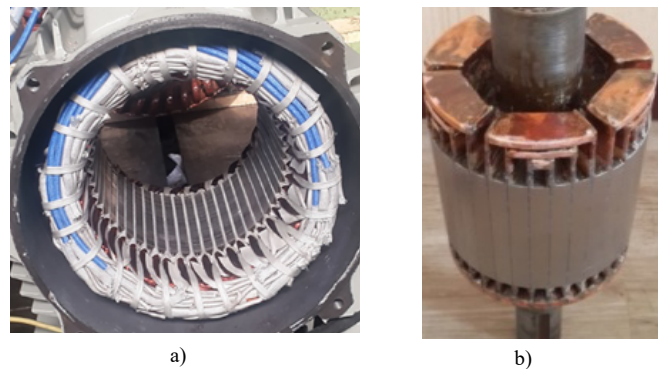


Fig. 5. The prototype BDFIM constructed: a) stator part, b) rotor part.

Fig. 6 shows the results obtained from the finite elements simulation at rated PW induction mode of operation. As shown, the flux density distribution confirms that no excessive saturation is presented in the iron, and the maximum flux density in different regions including the stator and rotor teeth and back iron are lower than the rated values. The analysis of the CW induction mode in FE simulation has also led to similar results.

To assess the harmonic content of the BDFIM when both stator PW and CW fields are presented, the prototype machine was modelled in cascade mode of operation where the CW was short circuited, and the PW was supplied at its rated conditions. Fig. 7 (a) shows the air gap magnetic flux

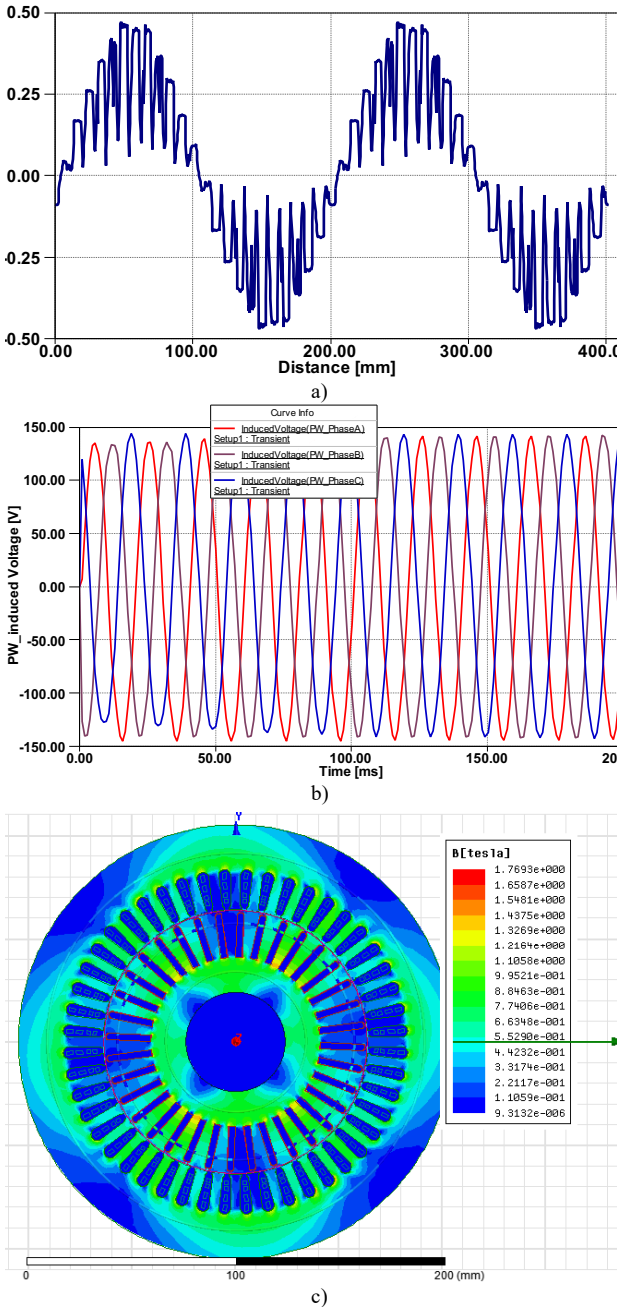


Fig. 6. Simulation results in no-load condition and PW induction mode: a) Air gap magnetic flux density distribution, b) PW induced voltages, c) 2D flux density distribution in the machine's magnetic circuit.

density in the air gap which includes the PW and CW fundamental components with 4 and 8 poles, respectively, as well as additional slot harmonics and stator time harmonics. Fig. 7 (b) shows the flux density distribution in the machine's magnetic circuit. The flux density is generally lower than the rated values in different parts of the stator and rotor magnetic circuits. The maximum flux density value observed in the iron circuit was 1.78 T located at the root of the rotor tooth, which is lower than the rated designed value of 1.8 T.

The harmonic spectrum of the air-gap flux density in the cascade mode is illustrated in Fig. 8. In addition to the 2nd and 4th fundamental components induced generated by the PW and CW fluxes, additional harmonic components such as

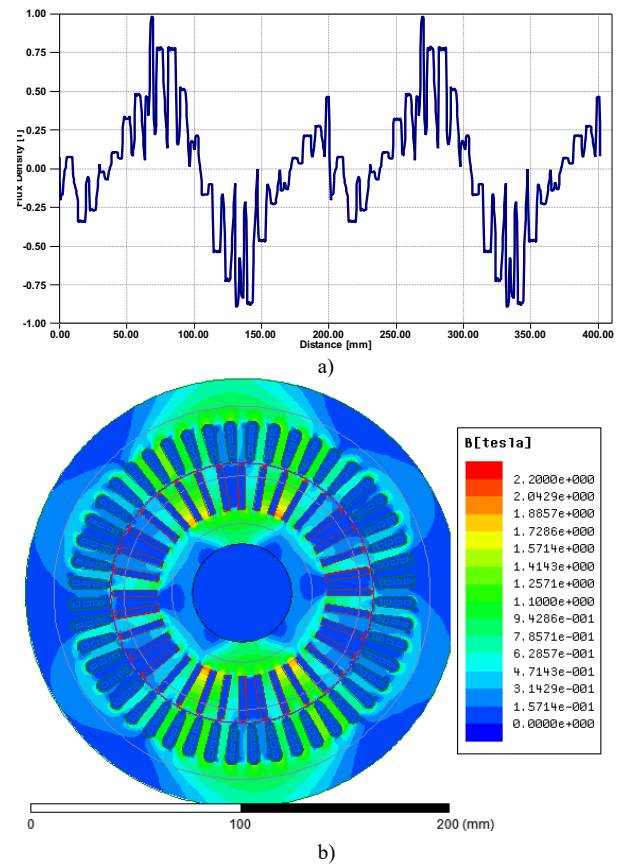


Fig. 7. Simulation results of cascade mode of operation: a) Magnetic flux density distribution in the air gap, b) 2D flux density distribution in the machine's magnetic circuit.

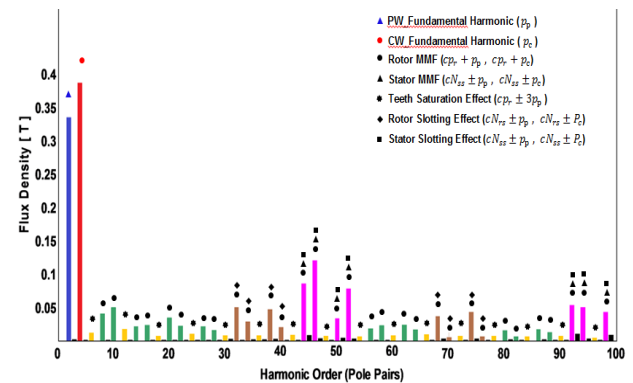


Fig. 8. Harmonic spectrum of air-gap flux density in cascade mode

rotor slot harmonics, saturation harmonics and the harmonics generated from the rotor and stator grooving can be observed. It is worth noting that in the cascade mode, the rotor core losses are significant and cannot be ignored. In [23] the improved steady-state model of this machine is presented taking into account the effects of the core losses. Furthermore, the accurate analysis of the real power flow in the machine is essential during the machine design process and the determination of the power converter's rating and its specifications [24].

VI. CONCLUSIONS

In this paper, the effective parameters for the BDFIM's design and their constraints were investigated. The design variables were determined based on the design objectives and to achieve an optimal design process. A BDFIM prototype was then constructed based on the parameters obtained from the optimal design process. To validate the design process, the experimental and finite elements simulation results were presented in induction and cascade modes of operation. The results showed close agreements between the finite element simulation and experimental tests. It was shown that in both induction and cascade modes, the flux density remains within the acceptable range and hence no excessive saturations were observed. Furthermore, the harmonic contents of the air gap magnetic field were assessed in cascade mode of operation showing the PW and CW fundamental fields as the dominant field components, as well as other harmonic components generated due to the stator and rotor slots effects and the time harmonics presented in stator windings. Future research will include more in-depth investigation of the field harmonics in the air gap as well as analysis of the machine in synchronous mode as the most desirable mode of operation to validate the proposed optimal design process at the machine's rated operating conditions.

VII. REFERENCES

- [1] S. Abdi, E. Abdi, H. Toshani, R. McMahon, "Vibration analysis of Brushless doubly fed machines in the presence of rotor eccentricity", *IEEE Transactions on Energy Conversion*, Vol. 35, pp. 1372-1380, 2020.
- [2] R. Sadeghi, S. Madani, "A New Smooth Synchronization of Brushless Doubly-Fed Induction Generator by Applying a Proposed Machine Model," *IEEE Trans. Sustain. Energy*, vol. 9, no. 1, pp. 371-380, Jan. 2018.
- [3] C. Brune, R. Spee, and A. K. Wallace, "Experimental evaluation of a variable-speed, doublyfedwind-power generation system," *IEEE Transactions on Industry Applications*, vol. 30, no. 3, pp. 648-655, 1993.
- [4] S. Shao, E. Abdi, and R. McMahon, "Stable operation of the Brushless Doubly-Fed Machine," *IEEE PEDS*, pp. 897-902, 2007.
- [5] K. Wallace, R. Spee, G. C. Alexander, "The brushless doubly-fed machine: Its advantages, applications and design methods," *IEE Conference on Electrical Machines and Drives*, pp.511-517, 1993.
- [6] H. K. Lauw, 1991, U.S. Patent No. 5, 028, 0804.
- [7] A. K. Wallace, and R. Spee, 1992, U.S. Patent No. 5, 083, 077.
- [8] F. Xiong, X. Wang, "Design of a Low-Harmonic-Content Wound Rotor for the Brushless Doubly Fed Generator," *IEEE Transaction On Energy Conversion*, vol. 29, no. 1, , pp. 158-168, March 2014.
- [9] P. J. Tavner, R.A. McMahon, P.C. Roberts, E. Abdi-Jalebi, X. Wang, M. Jagiela, and T. Chick, "Rotor Design & Performance for a BDFM," *XVII International Conference on Electrical Machines*, Greece, Sep 2006.
- [10] S. Abdi, A. Grace, E. Abdi, R. McMahon, "A new optimised rotor design for brushless doubly fed machines", *20th International Conference on Electrical Machines and Systems*, Australia, 2017.
- [11] S. Abdi, E. Abdi, A. Oraee, R. McMahon, "Investigation of magnetic wedge effects in large-scale BDFMs", *2nd IET Renewable Power Generation Conference*, China, 2013.

- [12] S. Abdi, E. Abdi, R. McMahon, "Numerical analysis of stator magnetic wedge effects on equivalent circuit parameters of brushless doubly fed machines", *XIII International Conference on Electrical Machines (ICEM)*, Greece, 2018.
- [13] H. Gorginpour, "Optimal Design of Brushless Doubly-Fed Induction Generator Considering Harmonic Effects for Maximizing Volumetric Power Density," Ph.D. dissertation, Sharif University of Technology, 2013.
- [14] E. Abdi-Jalebi, "Modeling and Instrumentation of Brushless Doubly-Fed (Induction) Machines," Ph.D. dissertation, University of Cambridge, 2006.
- [15] S. Tohidi, M. R. Zolghadri, H. Oraee, P. Tavner, E. Abdi and T. Logan, "Performance of the brushless doubly-fed machine under normal and fault conditions," *IET Electr. Power Appl.*, vol. 6, Iss. 9, pp. 621-627, July 2012.
- [16] I. Sarasola, J. Poza, M. Rodriguez, G. Abad, "Direct torque control design and experimental evaluation for the brushless doubly fed machine," *Energy Conversion and Management*, vol. 52, Iss. 2, pp. 1226-1234, Feb. 2011.
- [17] E.S. Hamdi, "Design of small electrical machines," vol. 13, Wiley, 1994.
- [18] S. Abdi, E. Abdi, R. McMahon, "A new iron loss model for brushless doubly-fed machines with hysteresis and field rotational losses", *IEEE Transactions on Energy Conversion*, Vol. 36, pp. 3221-3230, April 2021.
- [19] Y. Duan, and R. G. Harley, "A Novel Method for Multiobjective Design and Optimization of Three Phase Induction Machines," *IEEE Trans. Ind. Appl.*, vol. 47, no. 4, pp. 1707-1715, 2011.
- [20] H. A. Hosseinabadi, "Reliability model of wind turbine with Brushless doubly-fed induction generator," Ph.D. dissertation, Sharif University of Technology, 2010.
- [21] J. Pyrhonen, T. Jokinen, V. Hrabovcova, and H. Niemela, "DESIGN OF ROTATING ELECTRICAL MACHINES," John Wiley & Sons, Ltd. 2008.
- [22] P. C. Roberts, "A study of brushless doubly-fed (induction) machines," Ph.D. dissertation, University of Cambridge, 2005.
- [23] M. Yousefian, H. Abootorabi Zarchi, H. Gorginpour "Modified steady-state modelling of brushless doubly-fed induction generator taking core loss components into account", *IET Electric Power Applications* 13 (9), pp. 1402-1412, 2019.
- [24] M. Yousefian, H. Abootorabi Zarchi, H. Gorginpour "Accurate active power flow diagrams of Brushless doubly-fed induction machine in motoring and generating modes", *Springer, Electr Eng* vol. 102, pp. 1275-1286, 2020.

VIII. BIOGRAPHIES

M. Yousefian received the B.Sc. degree in electrical engineering from Shahid Rajaee University, Tehran, Iran, in 1999 and the M.Sc. and Ph.D. degrees in electrical engineering from Ferdowsi University of Mashhad, Iran, in 2004 and 2020, respectively. He is currently a faculty member at the Department of Electrical Engineering, Technical and Vocational University (TVU), Tehran, Iran, and a Consultant of Generator Fan Industrial Group. His research interests include electrical machine design and modeling, finite-element analysis, electric drives, and fault detection of electric machines.

H. Abootorabi Zarchi received the M.S. and Ph.D. degrees from the Isfahan University of Technology, Isfahan, Iran, in 2004 and 2010, respectively. He was a Visiting Ph.D. Student with the Control and Automation Group, Denmark Technical University, Denmark, from May 2009 to February 2010. He is currently an Assistant Professor in the Department of Electrical Engineering, Ferdowsi University of Mashhad, Mashhad, Iran. His research interests include electrical machines, nonlinear control of motor drives, and renewable energies.

S. Abdi received the B.Sc. degree in electrical engineering from Ferdowsi University, Mashhad, Iran, in 2009, the M.Sc. degree in electrical engineering from the Sharif University of Technology, Tehran, Iran, in 2011, and the Ph.D. degree in electrical machines design and optimisation from Cambridge University, Cambridge, U.K., in 2015. He is currently an Assistant Professor of electrical engineering with the University of East Anglia, Norwich, U.K. His main research interests include electrical machines and drives for renewable power generation and automotive applications.

H. Gorginpour received the B.Sc. degree in electrical engineering from Shiraz University, Shiraz, Iran, in 2007 and the M.Sc. and Ph.D. degrees in electrical engineering from Sharif University of Technology, Tehran, Iran, in 2009 and 2014, respectively. He is currently an Associate Professor at the Department of Intelligent Systems Engineering and Data Science, Persian Gulf University, Bushehr, Iran. His research interests include electrical machine design and modeling, finite-element analysis, and power electronics and drives.